NASA Technical Memorandum 84248
AVRADCOM Technical Report 82-A-7

NASA-TM-84248 19820019339

# Finite Difference Methods for the Solution of Unsteady Potential Flows

F. X. Caradonna

June 1982



National Aeronautics and Space Administration

United States Army Aviation Research and Development Command

NASA Technical Memorandum 84248

AVRADCOM Technical Report 82-A-7

# Finite Difference Methods for the Solution of Unsteady Potential Flows

F. X. Caradonna, Aeromechanics Laboratory
AVRADCOM Research and Technology Laboratories,
Moffett Field, California

NASA
National Aeronautics and
Space Administration

**Ames Research Center**
Moffett Field, California 94035

United States Army
Aviation Research and
Development Command
St. Louis, Missouri 63166

# FINITE DIFFERENCE METHODS FOR THE SOLUTION OF UNSTEADY POTENTIAL FLOWS

By

F. X. Caradonna,
Aeromechanics Laboratory, Army Research and Technology Laboratories (AVRADCOM), Ames Research Center, Moffett Field, CA. U.S.A. 94035

ABSTRACT

A brief review is presented of various problems which are confronted in the development of an unsteady finite difference potential code. This review is conducted mainly in the context of what is done for a typical small disturbance and full potential method. The issues discussed include choice of equations, linearization and conservation, differencing schemes, and algorithm development. A number of applications, including unsteady three-dimensional rotor calculations, are demonstrated.

ONE OF THE MOST IMPORTANT REALIZATIONS in fluid mechanics research was that transonic flow, for all its apparent complexity, is largely describable by potential theory. This fact was clouded by a thicket of problems concerning tunnel turbulence, wall and scaling effects, and separation. We now know that many of these problems are magnified by the inherent susceptibility of the inviscid transonic flow to unsteadiness. Of course, basic flow researchers were undoubtedly prejudiced in favor of potential theory from the outset because the inviscid, irrotational approximation is a tremendous simplification. Nevertheless, real progress did not occur until the explosive development of finite difference methods which occurred in the 1970's.

Spurred on by the promise of more cruise-efficient transport aircraft, our greatest progress has been in steady flow prediction. However, unsteady transonic flows are important because the aircraft structural response can induce large and heretofore unpredictable shock excursions. The flow on helicopter rotor tips is an even more interesting example of unsteady transonic flow. In this case, unsteadiness is not only forced by structural deformation but also by a free-stream flow which rapidly varies in speed and direction and contains large wake disturbances from previous blades. And so, unsteady transonic flow remains a rich mine of important problems waiting to be solved. Potential methods will probably play a dominant role in this process — not only because of validity but also because it promises to be the most efficient method.

Efficiency is a more important matter for unsteady computations than for the steady case. This is because we require the resolution of physical time and do not have the benefit of acceleration methods that are used in steady problems. In general, however, the unsteady and steady methods are much the same. At present, the most versatile and efficient unsteady methods are two- and three-dimensional small disturbance codes, but full potential methods are currently under rapid development. The following discussion will review many of the important algorithm and code development issues in the context of small disturbance and full potential methods.

## FORMULATIONS OF THE PROBLEM

The starting point for the various potential formulations is the mass conservation and Bernoulli's equation (shown here for an inertial reference frame)

$$\rho_t + \nabla \cdot (\rho \nabla \phi) = 0 \tag{1}$$

$$\frac{\rho}{\rho_\infty} = \left\{ 1 - \frac{\gamma-1}{c_\infty^2} \left[ \phi_t + \frac{1}{2} (\nabla\phi)^2 \right] \right\}^{\frac{1}{r-1}} \tag{2}$$

These equations have the advantage (when combined) that only one flow variable, $\Phi$, need be solved for. However, these equations are only an approximation to the exact inviscid equations because they assert that mass, energy and entropy are conserved throughout the flow field. The component of momentum normal to any shock is not conserved in this approximation

(1,2)*. This is a notable difference from the Rankine-Hugoniot equations where shock drag comes about through the change in entropy across the shock. The error thus induced is generally not excessive until shock strengths are attained that involve separation and the necessity to abandon the inviscid approximation. Conservative formulations are required to closely approximate Rankine-Hugoniot results. Nevertheless, nonconservative formulations are still actively employed, due to the happy accident that errors of conservation frequently have an effect similar to boundary-layer corrections on shock location.

In attacking a given problem it is first necessary to express Eqs. (1) and (2) in the relevant body-fixed coordinate system for the problem to be solved. The transformation (3) which encompasses both wings or rotors in edgewise motion is

$$\vec{r}' = \vec{U}_\infty t + R(t)\vec{r}$$
$$t' = t \tag{3}$$

where $r' = (x',y',z')$ and $r = (x,y,z)$ are the inertial and body-fixed coordinates (see Fig. 1), respectively, and $R(t)$ is the rotation matrix

$$R(t) = \begin{bmatrix} \cos \Omega t & -\sin \Omega t & 0 \\ \sin \Omega t & \cos \Omega t & 0 \\ 0 & 0 & 1 \end{bmatrix}$$

(Note that for no rotation, $\Omega = 0$, Eq. (3) reduces to the usual Galilean transformation.) Under this transformation, Eqs. (1) and (2) become

$$\rho_t + \nabla \cdot \left[\rho \vec{V}\right] \tag{4}$$

$$\frac{\rho}{\rho_\infty} = \left\{1 - \frac{\gamma-1}{c_\infty^2}\left[\phi_t + \frac{1}{2}\left(V^2 - a^2\right)\right]\right\}^{\frac{1}{\gamma-1}} \tag{5}$$

where $\vec{a} = U_\infty(\vec{i}\cos\Omega t - \vec{j}\sin\Omega t) - \vec{\Omega} \times \vec{r}$ is the undisturbed free-stream velocity seen by an observer in body-fixed coordinates and

$$\vec{V} = \vec{a} + \nabla\phi \tag{6}$$

is the flow velocity seen in the moving coordinates. A common misunderstanding concerns the validity of potential theory where rotary motion is involved. In fact, the motion of the coordinates, $-\vec{a}$, has no bearing on whether or not a potential exists. However, since $\vec{a}$ need not be an irrotational function, $\vec{V}$ is not generally expressible as the gradient of a full potential. Rather, $\phi$ defines a disturbance about $\vec{a}$, as seen in Eq. (6).

*Numbers in parentheses designate References at end of paper.

Equations (4) and (5) are here written for a generalized, moving coordinate system $\xi,\eta,\zeta,\tau$ where

$$\begin{aligned}\xi &= \xi\,(x',y',z',t)\\ \eta &= \eta\,(x',y',z',t)\\ \zeta &= \zeta\,(x',y',z',t)\\ \tau &= t\end{aligned}$$

giving

$$\partial_\tau(\rho/J) + \partial_\xi(\rho U/J) + \partial_\eta(\rho V/J) + \partial_\zeta(\rho W/J) = 0 \tag{4a}$$

where

$$U = \xi_t + \nabla\xi \cdot (\phi_\xi \nabla\xi + \phi_\eta \nabla\eta + \phi_\zeta \nabla\zeta)$$

$$V = \eta_t + \nabla\eta \cdot (\phi_\xi \nabla\xi + \phi_\eta \nabla\eta + \phi_\zeta \nabla\zeta)$$

$$W = \zeta_t + \nabla\zeta \cdot (\phi_\zeta \nabla\xi + \phi_\eta \nabla\eta + \phi_\zeta \nabla\zeta)$$

are here the contravariant velocity components and have the form of Eq. (6), $J$ is the Jacobian $|\partial(\xi,\eta,\zeta)/\partial(x',y',z')|$ and $\nabla$ is the cartesian gradient operator. In the same manner, Bernoulli's equation becomes in these coordinates

$$\rho = \left\{1 - \frac{(\gamma-1)}{2}\left[2(\phi_\tau + \xi_t\phi_\xi + \eta_t\phi_\eta + \zeta_t\phi_\zeta) + (\xi_x\phi_\xi + \eta_x\phi_\eta + \zeta_x\phi_\zeta)^2 + (\xi_y\phi_\xi + \eta_y\phi_\eta + \zeta_y\phi_\zeta)^2 + (\xi_z\phi_\xi + \eta_z\phi_\eta + \zeta_z\phi_\zeta)^2\right]\right\}^{\frac{1}{\gamma-1}} \tag{5a}$$

where we use the nondimensionalizations $\tilde{\rho} \to \rho/\rho_\infty$, $\tilde{x} \to x/\ell$, $\tilde{y} \to y/\ell$, $\tilde{z} \to z/\ell$, $\tilde{\phi} \to \phi/\ell c_\infty$, and $\tau \to tc_\infty/\ell$, and the tilda is suppressed. Here, $\ell$ is a reference length such as the airfoil chord.

SMALL DISTURBANCE EQUATIONS--The classical small disturbance derivation involves substituting Eq. (5) into Eq. (4) to eliminate $\rho$. The resulting equation is nondimensionalized, scaled, and higher order terms are eliminated, subject to the limit process that $(1-M^2)/\delta^{2/3} = O(1)$ as $M \to 1$ and $\delta \to 0$. The resulting equation takes the form,

$$A\phi_{tt} + B\phi_{xt} = F_x + \phi_{zz} + C\phi_{yy} + D\phi_{xy} \tag{7}$$

where

$\phi \to \phi/U_c \ell \delta^{2/3}$

$\Omega$ = frequency of unsteady motion (the rotation rate for a rotor)

$M = U_c/c_\infty$, a characteristic Mach number

$U_c$ = characteristic speed ($V_\infty$ for a wing, $\Omega R$ for a rotor)

$AR = R/\ell$, aspect ratio

$k = \Omega\ell/U_c$, reduced frequency (for a rotor $k = 1/AR$)

$\delta$ = blade thickness ratio

$A = M^2k^2/\delta^{2/3}$

$B = 2M^2kf/\delta^{2/3}$

$C = 1/AR^2\delta^{2/3}$

$D = Bg$

$f = y + \mu\cos t$ (for rotor), or 1 (for a wing)

$$F = \frac{1-f^2M^2}{\delta^{2/3}}\phi_x - M^2\left[\left(\frac{\gamma+1}{2}\right)f\phi_x + (\gamma-1)k\phi_t\right]\phi_x$$

$g = x + \sin t$ (rotor), or 1 (wing)

$\mu = \Omega R/V_\infty$, rotor advance ratio

$t = \Omega t'$

$x = x'/\ell$

$y = y'/R$ (R is either a rotor radius or the wing span of a fixed wing)

$$z = \frac{z'\delta^{1/3}}{\ell}$$

$\ell$ = chord

Equation (7) is not unique and an assortment of modifications and additions have been made to improve its ability to handle oblique shocks (see Ref. 4). Nevertheless, they all have the same general form and have essentially identical unsteady terms.

The pressure coefficient in the small disturbance approximation is given by

$$C_p = \frac{P - P_\infty}{\frac{1}{2}\rho U_c^2} = -2f\delta^{2/3}(\phi_x + k\phi_\tau) \tag{8}$$

The body surface boundary condition is the familiar slope condition applied at a mean surface,

$$\phi_z = f(kb_t + b_x) \tag{9}$$

where the body surface is described by $z = \delta b(x,y,t)$.

There is an additional boundary condition that pressure be continuous across the stagnation streamline behind and on the trailing edge of an airfoil (Kutta condition). Using Eq. (8), this condition is expressed as

$$\Gamma_x + k\Gamma_t = 0 \qquad \text{where} \quad \Gamma \equiv [\![\phi]\!] \tag{10}$$

This equation expresses the downstream convection of vorticity (or the potential discontinuity). It happens that $\phi_{zz}$ is also discontinuous in the airfoil wake. This is seen by applying Eq. (7) (in linearized form) across the wake and substituting Eq. (10) to obtain

$$\chi = [\![\phi_{zz}]\!] = -\left[\alpha + \frac{1}{k}\left(B - \frac{A}{k}\right)\right]\Gamma_{xx} - C\Gamma_{yy} \tag{11}$$

where

$$\alpha = \frac{1 - f^2M^2}{\delta^{2/3}}$$

This quantity, $\chi$, is zero only in steady two-dimensional flow or steady nonlifting three-dimensional flow.

Finally, finite difference methods require far-field boundary conditions. Typically, one specifies some combination of $\phi = 0$, $\phi_n = 0$, or $C_p = 0$ on the outer boundaries and subsequently relies upon a large boundary distance (often over $100\ell$) to dissipate the ensuing wave reflections. However, it has been shown that good approximate nonreflecting boundary conditions can be constructed (5-8). For example, consider Eq. (7) in its two-dimensional, linearized form

$$A\phi_{tt} + B\phi_{xt} = \alpha\phi_{xx} + \phi_{zz}$$

The wave information for a plane wave, $\hat{\phi} = e^{i(\omega t+\xi x+\zeta z)}$, must satisfy

$$A\omega^2 + B\omega\xi = C\xi^2 + \zeta^2$$

A condition which prevents reflection of upstream-moving waves at the front grid boundary is

$$\omega = \frac{-B\xi + \sqrt{(B^2+4A\alpha)\xi^2 - 4A\eta^2}}{2A}$$

This expression does not transform back to a simple local differential operator. However, in the limit $\eta/\xi \to 0$ (for wavefronts parallel to the upstream boundary) we obtain the expression

$$\omega \approx \left(\frac{\sqrt{B^2+4A\alpha} - B}{2A}\right)\xi$$

whose inverse Fourier transformation yields

$$\phi_t = \frac{\sqrt{B^2+4A\alpha} - B}{2A}\,\phi_x \tag{12}$$

Similar expressions can be obtained for all boundary faces.

Although its limitations are many and well known, the small disturbance approximation (with judicious use) often gives excellent results and remains in active use. Perhaps the greatest importance of small disturbance theory is that it contains (in simplified form) all the important issues contained in the full equations and hence constitutes a good testing ground for future techniques. There is, perhaps, one exception to this statement. It concerns the fact that when Eqs. (4) and (5) are combined to produce a single equation for $\phi$, a nonconservative formulation results. This problem does not occur in classical small disturbance theory.

FULL POTENTIAL EQUATIONS—For computational efficiency, we usually seek to formulate the potential equations so that we need only one dependent variable. This is easily done, since Eq. (4) can be rewritten as

$$\frac{\partial\rho}{\partial\Phi}\frac{\partial\Phi}{\partial t} + \rho\left(\frac{\partial^2\Phi}{\partial x^2} + \frac{\partial^2\Phi}{\partial y^2} + \frac{\partial^2\Phi}{\partial z^2}\right) + \Phi_x\frac{\partial\rho}{\partial\Phi}\frac{\partial\Phi}{\partial x} + \Phi_y\frac{\partial\rho}{\partial\Phi}\frac{\partial\Phi}{\partial y} + \Phi_z\frac{\partial\rho}{\partial\Phi}\frac{\partial\Phi}{\partial z} = 0$$

where

$$\frac{\partial\rho}{\partial\Phi} = -\rho^{2-\gamma}\left(\frac{\partial}{\partial t} + \Phi_x\frac{\partial}{\partial x} + \Phi_y\frac{\partial}{\partial y} + \Phi_z\frac{\partial}{\partial z}\right) \tag{13}$$

is a noncommuting differential operator. For this equation we assume the nonlinearizations pertaining to Eq. (5) (for the previous and following equations we assume pure translational motion). On applying the isentropic relations we obtain the familiar textbook form of the potential equation

$$\Phi_{tt} + 2u\Phi_{xt} + 2v\Phi_{yt} = (c^2-u^2)\Phi_{xx} + (c^2-v^2)\Phi_{yy} + (c^2-w^2)\Phi_{zz} - 2\Phi_x\Phi_y\Phi_{xy} - 2\Phi_x\Phi_z\Phi_{xz} - 2\Phi_y\Phi_z\Phi_{yz} \tag{14}$$

The problem arises, however, that equation (14) cannot be brought back into conservation law form with $\phi$ retained as the dependent variable.

In examining Eq. (4) we see that $\rho$ presents no problem in the spacial derivative terms because it can be evaluated from the previous time step (that is, it is taken as the leading term in a Taylor series in time). The required implicit spacial terms involving $\Phi$ then come about through $\vec{V}$. What is required is a way to obtain a conservative temporal function of $\Phi$ from the $\rho_t$ term. This can be accomplished through the following linearization,

$$\rho = \rho_o + \left(\frac{\partial\rho}{\partial\Phi}\right)_o(\Phi-\Phi_o) \tag{15}$$

where the subscript, o, denotes a nearby known state or solution. With this expansion the density time derivative becomes

$$\rho_t \rightarrow \frac{\partial}{\partial t}\left(\left(\frac{\partial\rho}{\partial\Phi}\right)_o\Phi\right) + \frac{\partial}{\partial t}\left(\rho_o - \left(\frac{\partial\rho}{\partial\Phi}\right)_o\Phi_o\right) \tag{16}$$

which provides a conservative time-differenced function of $\Phi$ (9,10).

The above linearization can be avoided for a conservative formulation only if one is willing to retain two dependent variables. This approach has been taken by Chipman and Jameson (11) who solve the first-order system consisting of the mass conservation equation and Bernoulli's equation rewritten in the form

$$\Phi_t + h(\rho, \nabla\Phi, c_\infty) = 0$$

SPACIAL DIFFERENCING

The primary stability issue in transonic finite difference problems (steady or unsteady) concerns proper spacial differencing in the subsonic and supersonic flow regions. Consider first the simple steady two-dimensional model problem

$$(1-M_\infty^2)\,\phi_{xx} + \phi_{yy} = 0 \tag{17}$$

and let the difference operators $\nabla_x, \Delta_x, \nabla_y$, and $\Delta_y$ be defined as $\nabla_x\phi = (\phi_i + \phi_{i-1})/\Delta x$, $\Delta_x\phi = (\phi_{i+1} - \phi_i)/\Delta x$, etc. It is well known that the following difference schemes

$$(1-M_\infty^2)\,\nabla_x\Delta_x\phi + \nabla_y\Delta_y\phi = 0 \quad , \quad M_\infty < 1 \tag{18a}$$

$$(1-M_\infty^2)\,\nabla_x\nabla_x\phi + \nabla_y\Delta_y\phi = 0 \quad , \quad M_\infty > 1 \tag{18b}$$

are, respectively, suitable for the above model elliptic and hyperbolic problems. The differencing equation (Eq. 18b) is divergent if $M_\infty < 1$ while (Eq. 18a) is convergent for $M_\infty > 1$ only if $\left|\Delta x/[(1-M_\infty^2)\,\Delta y]\right| \leq 1$, an impractical restriction as $M_\infty \to 1$. Murman and Cole (12), aware of these constraints, introduced type-dependent differencing for the transonic small disturbance equation. In this approach the streamwise spatial difference operator is either central or backward, depending on the local Mach number.

In order to obtain a stable conservative streamwise difference operator for Eq. (7), it is first necessary to time-linearize the nonlinear flux term F. One way to do so (13) is

$$F^{n+1} = F^n + \left(\frac{\partial F}{\partial \phi_x}\right)^n \left(\phi_x^{n+1} - \phi_x^n\right) + \left(\frac{\partial F}{\partial \phi_t}\right)^n \left(\phi_t^{n+1} - \phi_t^n\right)$$

This time-linearized flux is differenced and defined at each midcell of the computational grid as

$$F_{i+\frac{1}{2}}^{n+1} = F_{i+\frac{1}{2}}^{n} + \left(\frac{\partial F}{\partial \phi_x}\right)^n \Delta_x(\phi^{n+1} - \phi^n) + \left(\frac{\partial F}{\partial \phi t}\right)^n \nabla_t(\phi^{n+1} - \phi^n)$$

where

$$F^{n}_{i+\frac{1}{2}} = \alpha\Delta_x\phi^n - M^2\left[\left(\frac{\gamma+1}{2}\right)f\Delta_x\phi^n + k(\gamma-1)\nabla_t\phi^n\right]\Delta_x\phi^n$$

$$\left(\frac{\partial F}{\partial \phi_x}\right)^n = \alpha - M^2\left[(\gamma+1)f\Delta_x\phi^n + k(\gamma-1)\nabla_t\phi^n\right]$$

and

$$\left(\frac{\partial F}{\partial \phi_t}\right)^n = -M^2(\gamma-1)k\Delta_x\phi^n$$

For this flux operator Murman's conservative switching scheme (14) is

$$F_x \rightarrow D_x F \equiv \frac{1}{\Delta x}\left[\varepsilon_i(F_{i+\frac{1}{2}}-F_{i-\frac{1}{2}}) + (1-\varepsilon_{i-1})(F_{i-\frac{1}{2}}-F_{i-3/2})\right] \qquad (19)$$

where

$$\varepsilon_i = \begin{cases} 1 & , \quad M_i > 0 \\ 0 & , \quad M_i < 0 \end{cases}$$

and

$$M_i = \alpha - M^2(\gamma+1)\phi_x - M^2(\gamma-1)k\phi_t$$

Note that for greater time accuracy, the Crank-Nicolson time averaging of spacial operators is often applied. For instance, we could define the flux term $\tilde{F} = (F^{n+1} + F^n)/2$ and subsequently apply the above linearization and switching scheme.

The nonconservative full potential equation (Eq. 14) can be type-differenced in a manner very similar to that of the small disturbance equation. Equation (14) can be rearranged in the cannonical form (15,16)

$$\phi_{tt} + 2q\phi_{st} = (c^2-q^2)\phi_{ss} + c^2\phi_{nn} \qquad (20)$$

where $s$ is a coordinate locally aligned to the stream direction and $n$ is a normal coordinate. For the two-dimensional case

$$\phi_{nn} = \frac{1}{q^2}(v^2\phi_{xx} + 2uv\phi_{xy} + u^2\phi_{yy})$$

$$\phi_{ss} = \frac{1}{q^2}(u^2\phi_{xx} + 2_{uv}\phi_{xy} + v^2\phi_{yy})$$

and

$$2q\phi_{st} = 2u\phi_{xt} + 2v\phi_{yt}$$

It is seen that the steady part of Eq. (20) has the same form as Eq. (18). Therefore a stable scheme results when $\phi_{nn}$ is always central-differenced and $\phi_{ss}$ is type-differenced based on the sign of $c^2 - q^2$.

This assertion of stability, by analogy to known stable methods, can be applied to the full potential equation. For this case we require the following difference scheme for the model equation, Eq. (17).

$$\nabla_x \Delta_x \phi - M_\infty^2 \nabla_x \nabla_x \phi + \nabla_y \Delta_y \phi = 0 \tag{21}$$

This scheme, though less accurate than Eq. (18a), is stable for the entire Mach number range with no need to switch difference operators.

Now consider the spatial derivative term $\partial_x \rho \phi_x$ of Eq. (4). A local linearization of this term gives

$$\partial_x \rho \phi_x = \partial_x \left[ \left( \rho \phi_x \right)_o + \left( \phi_x \frac{\partial \rho}{\partial \phi} + \rho \frac{\partial}{\partial x} \right)_o (\phi - \phi_o) \right] \tag{22}$$

which upon substitution of Eq. (13) and assumption of steady small disturbance flow yields the approximate expression,

$$\partial_x (\rho \phi_x) \doteq \partial_x (\rho_o \phi_x) - \partial_x \left[ \left( \frac{\rho u^2}{c^2} \right)_o \phi_x \right] \tag{23}$$

If we further assume $\rho_o$ and $(u/c)_o$ to be spacially constant we have

$$\partial_x (\rho \phi_x) \doteq \rho \left[ \phi_{xx} - M^2 \phi_{xx} \right] \tag{24}$$

which demonstrates an approximate equivalence between the full potential equation and the model Eq. (17). The importance of Eq. (24) is that the origin of the second $\phi_{xx}$ on the right-hand side is in the evaluation of $\rho$ from Bernoulli's equation. Therefore, the differencing scheme of Eq. (21) is significant because it is roughly equivalent to evaluating $\partial_x \rho \phi_x$ with a centered scheme employing an upstream biased $\rho$. The stability of this density biasing has been demonstrated in Refs. (17-19). This density biasing will be expanded upon in the following section.

## NUMERICAL ALGORITHMS

The final step in a finite difference solution scheme is the efficient solution of the system of algebraic equations which result from the various discretizations. Because these systems are all too large to be solved efficiently (in spite of their sparseness), it is necessary to reduce them to a more manageable form. All the unsteady schemes today use some sort of approximate factorization. That is, the system matrix is replaced by a product of easily solved submatrices. In general, this product is not equal to the original system matrix. However, it is possible to keep the discrepancies within the bounds of the discretization error.

SMALL DISTURBANCE EQUATION—The germ of the approximate factorization idea is quite old, having been first expressed in the ADI method. A typical ADI scheme for Eq. (7) is

$$\text{Step 1.} \quad \frac{B}{\Delta t} \nabla_x (\tilde{\phi} - \phi^n) = D_x F(\tilde{\phi}) + C \nabla_y \Delta_y \phi^n + \nabla_z \Delta_z \phi^n + D \nabla_x \begin{cases} \nabla_y \phi^n & , \quad D < 0 \\ \Delta_y \phi^n & , \quad D > 0 \end{cases}$$

$$\text{Step 2.}\quad \frac{B}{\Delta t}\nabla_x(\tilde{\tilde{\phi}}-\phi^n) = D_xF(\tilde{\phi}) + C\nabla_y\Delta_y\phi^n + \nabla_z\Delta_z\phi^n + D\nabla_x\begin{Bmatrix}\nabla_y\tilde{\tilde{\phi}} & , & D<0\\ \Delta_y\tilde{\tilde{\phi}} & , & D>0\end{Bmatrix}$$

$$\text{Step 3.}\quad A\nabla_t\nabla_t\phi^{n+1} + B\nabla_t\nabla_x\phi^{n+1} = D_xF(\tilde{\phi}) + C\nabla_y\Delta_y\tilde{\tilde{\phi}} + \nabla_z\Delta_z\phi^{n+1} + D\nabla_x\begin{Bmatrix}\nabla_y\tilde{\tilde{\phi}} & , & D<0\\ \Delta_y\tilde{\tilde{\phi}} & , & D>0\end{Bmatrix}$$

Note that the cross derivative term is treated implicitly and is always an upwind difference (20,21). The advantage of this ADI scheme is that each step involves a simple matrix inversion (steps 2 and 3 require a tridiagonal and step 1 requires a quadradiagonal inversion). Note also that these steps are written so as to maximize their similarity to Eq. (7). However, they are never actually solved in this form. It is more efficient to subtract steps 1 and 2 from steps 2 and 3, respectively, and solve the resulting equations. The insertion of the $\phi_{tt}$ discretization in the above algorithm is very convenient and was first introduced by Rizetta and Chen (22).

It can be shown that the above ADI scheme constitutes a product of terms which are a good approximation to the original difference equation. This scheme was originally devised with the idea that each step should be a consistent approximation of the original difference equation. However, if this constraint is relaxed there are a number of factorizations which can be found. To see how this is done, consider the model equation

$$\phi_{xt} = \beta\phi_{xx} + \phi_{yy}$$

which is differenced as

$$\nabla_t\nabla_x\phi^{n+1} = \beta\nabla_x\Delta_x\phi^{n+1} + \nabla_y\Delta_y\phi^{n+1} \quad (\text{for } \beta > 0)$$

and then rearranged as

$$(\nabla_x-\beta\nabla_x\Delta_x-\nabla_y\Delta_y)\phi^{n+1} = \nabla_x\phi^n \quad .$$

The left-hand side of this equation can be approximated by the product $(1-\beta\Delta_x)(\nabla_x-\nabla_y\Delta_y)$ if the error term $\beta\nabla_x\Delta_y\nabla_y$ is eliminated. This elimination is easily accomplished using the known information at step $n$. And so, an appropriate approximate factorization (commonly called the AF2 scheme) is

$$(1-\beta\nabla_x)(\nabla_x-\nabla_y\Delta_y)\phi^{n+1} = (\nabla_x+\beta\Delta_x\nabla_y\Delta_y)\phi^n$$

This gives rise to a two-step procedure — one step being a bi-diagonal and the other a tri-diagonal inversion. A further simplification is to solve for $(\phi^{n+1}-\phi^n)$ rather than $\phi^{n+1}$ in order to simplify the evaluation of the right-hand side.

CONSERVATIVE FULL POTENTIAL METHOD—The above factorization approach will now be applied to the unsteady full potential equation. We will first derive a simplified form of the equation for two dimensions. Consider Eqs. (4) and (5) in their two-dimensional form subject to the mapping $\xi = \xi(x), \eta = \eta(x)$ and assume a steady free-stream motion allowing $\phi$ to be expressed as $\phi \rightarrow M_\infty x + \phi$. This gives

$$\partial_t(\rho/J) + \partial_\xi\left(\frac{\rho\xi_x^2}{J}\phi_\xi\right) + \partial_\eta\left(\frac{\rho\eta_z^2}{J}\phi_\eta\right) = 0 \tag{25a}$$

$$\rho = \left\{1 - (\gamma-1)\left[\phi_\tau + \frac{1}{2}\left(\xi_x^2\phi_\xi^2 + \eta_y^2\phi_y^2 - M_\infty^2\right)\right]\right\}^{\frac{1}{\gamma-1}} \tag{25b}$$

On application of the linearization of Eq. (15), Eq. (25a) is differenced as

$$\begin{aligned}\nabla_t\left[\hat{\beta}^n(\nabla_t + \xi_x^2\phi_\xi\delta_\xi + \eta_z^2\phi_\eta\delta_\eta)(\phi^{n+1} - \phi^n)\right] &= \bar{\delta}_\xi(\hat{\rho}^n\xi_x^2\delta_\xi\phi^{n+1}) \\ &+ \bar{\delta}_\eta(\hat{\rho}^n\eta_z^2\delta_\eta\phi^{n+1}) + \nabla_t\rho^n\end{aligned} \tag{26}$$

where $\beta \equiv \rho^{2-\gamma}$, $\hat{}$ implies division by $J$, and the reference state 0 is now taken to be the previous time step $n$. The spacial operators in Eq. (26) are defined as

$$\delta_\xi = \frac{(\ )_{i+1} - (\ )_{i-1}}{2} \tag{27a}$$

$$\delta_\eta = \frac{(\ )_{i+1} - (\ )_{i-1}}{2} \tag{27b}$$

$$\begin{aligned}\bar{\delta}_\xi(\hat{\rho}\xi_x^2\delta_\xi\phi) = &\left(\frac{\xi_x^2}{J}\right)_{i+\frac{1}{2}}\left[(1-\nu_{i+1})\frac{\rho_{i+1}+\rho_i}{2}\right. \\ &\left.+ \nu_{i+1}\frac{(1+\theta)\rho_i + (1-\theta)\rho_{i-1}}{2}\right](\phi_{i+1} - \phi_i) \\ &-\left(\frac{\xi_x^2}{J}\right)_{i-\frac{1}{2}}\left[(1-\nu_i)\frac{\rho_i + \rho_{i-1}}{2}\right. \\ &\left.+ \nu_i\frac{(1+\theta)\rho_{i-1} + (1-\theta)\rho_{i-2}}{2}\right](\phi_i - \phi_{i-1})\end{aligned} \tag{27c}$$

$$\bar{\delta}_\eta(\hat{\rho}\eta_z^2\,\bar{\delta}_\eta\phi) = \left(\frac{\eta_z^2}{J}\right)_{j+\frac{1}{2}} \frac{\rho_{j+1}+\rho_j}{2}(\phi_{j+1}-\phi_j)$$

$$-\left(\frac{\eta_z^2}{J}\right)_{j-\frac{1}{2}} \frac{\rho_j+\rho_{j-1}}{2}(\phi_j-\phi_{j-1}) \qquad (27d)$$

Here, $\Delta\xi = \Delta\eta = 1$ and only the varying indices are indicated. The parameter $\theta = 1$ or 2 for first- or second-order spatial accuracy in supersonic regions. The switching parameter $\nu$ is defined in a way similar to (17) as

$$\left.\begin{aligned} &\nu = [1-(\rho/\rho^*)^2]c \quad 1 \le c < 10 \\ &\nu \equiv 0 \quad \text{if} \quad \nu < 0 \ \text{(i.e., subsonic)} \\ &\nu \equiv 1 \quad \text{if} \quad \nu > 1 \ \text{(i.e., supersonic)} \end{aligned}\right\} \qquad (28)$$

where $\rho^*$ is density evaluated at sonic conditions.

The parameter $\nu$ can be set to 1 throughout, but accuracy will be impaired unless $\theta$ is also set to 2. The operators in Eqs. (27a) and (27b) assume that the flow will be supersonic only in the positive x-direction. The density is found from the Bernoulli equation with ($\Delta\xi = \Delta\eta = 1$):

$$\phi_\xi\Big|_i \doteq \frac{\phi_{i+1}-\phi_{i-1}}{2} = \delta_\xi\phi_i$$

$$\phi_\eta\Big|_j \doteq \frac{\phi_{j+1}-\phi_{j-1}}{2} = \delta_\eta\phi_j$$

$$\phi_\tau\Big|^{n+1} \doteq \frac{(\phi^{n+1}-\phi^n)}{\Delta t} = \delta_\tau\phi^{n+1}$$

The metrics $\xi_x$ and $\eta_z$ are obtained from

$$\xi_x = \frac{2}{x_{i+1}-x_{i-1}}$$

$$\eta_y = \frac{2}{z_{j+1}-z_{j-1}}$$

while the term $(\xi_x^2/J)_{i+\frac{1}{2}}$ in Eq. (26) is formed either as

$$\left(\frac{\xi_x^2}{J}\right)_{i+\frac{1}{2}} = \frac{(\xi_x^2/J)_{i+1}+(\xi_x^2/J)_i}{2} \qquad (29a)$$

or

$$\left(\frac{\xi_x^2}{J}\right)_{i+\frac{1}{2}} = \frac{(\xi_x/J)_{i+1} + (\xi_x/J)_i}{2(x_{i+1} - x_i)} \tag{29b}$$

The terms $(\xi_x^2/J)_{i-1/2}$, $(\eta_z^2/J)_{j+1/2}$, and $(\eta_z^2/J)_{j-1/2}$ receive similar treatment. If Eq. (19a) is used, it is essential to add $-\delta_\xi(\rho_\infty \xi_x^2/J)\bar{\delta}_\xi \Phi_\infty$ to the right-hand side of Eq. (16) to subtract out a numerical truncation error due to incomplete metric cancellation.

Eq. 26 is now rearranged into delta form; it is now to be solved for $\Delta\phi = \phi^{n+1} - \phi^n$. For example, the term $\bar{\delta}_\xi(\xi_x^2 \hat{\rho}^n)\bar{\delta}_\xi \phi^{n+1}$ can be rearranged as

$$\bar{\delta}_\xi(\xi_x^2 \hat{\rho}^n)\bar{\delta}_\xi(\Delta\phi) + \bar{\delta}_\xi(\xi_x^2 \hat{\rho}^n)\bar{\delta}_\xi \phi^n$$

When the equation is put into delta form all the unknown terms are arranged together, resulting in

$$\begin{aligned}
&\Big((\beta^n/J^{n+1})\left[\delta_\tau + (\xi_x^2)^{n+1}\phi_\xi^n\delta_\xi + (\eta_y^2)^{n+1}\phi_\eta^n\delta_\eta\right] - h\bar{\delta}_\xi(\xi_x^2/J)^{n+1}\rho^n\bar{\delta}_\xi \\
&- h\bar{\delta}_\eta(\eta_y^2/J)^{n+1}\rho^n\bar{\delta}_\eta\Big)(\phi^{n+1} - \phi^n) \\
&= (\beta^{n-1}/J^n)\left[\delta_\tau + (\xi_x^2)^n\phi_\xi^{n-1}\delta_\xi + (\eta_y^2)^n\phi_\eta^{n-1}\delta_\eta\right](\phi^n - \phi^{n-1}) \\
&\quad + (\hat{\rho}^n - \hat{\rho}^{n-1}) + h\Big(\bar{\delta}_\xi(\xi_x^2/J)^{n+1}\rho^n\bar{\delta}_\xi\phi^n \\
&\quad + \bar{\delta}_\eta(\eta_y^2/J)^{n+1}\rho_n\delta_n\phi^n\Big)
\end{aligned} \tag{30}$$

which can be approximately factored into the form

$$\begin{aligned}
&\{I + \Delta t(\eta_y^2)^{n+1}\phi_\eta^n\delta_\eta - \Delta t(J^{n+1}/\beta^n)h\bar{\delta}_\eta(\eta_y^2/J)^{n+1}\rho^n\bar{\delta}_\eta\}_x \\
&\{I + \Delta t(\xi_x^2)^{n+1}\phi_\xi^n\delta_\xi - \Delta t(J^{n+1}/\beta^n)h\bar{\delta}_\xi(\xi_x^2/J)^{n+1}\rho^n\bar{\delta}_\xi\}(\phi^{n+1} - \phi^n) \\
&= [1 + (\beta^{n-1}/\beta^n)(J^{n+1}/J^n)](\phi^n - \phi^{n-1}) - (\beta^{n-1}/\beta^n)(J^{n+1}/J^n)(\phi^{n-1} - \phi^{n-2}) \\
&\quad + \Delta t(\beta^{n-1}/\beta^n)(J^{n+1}/J^n)\left[(\xi_x^2)^n\phi_\xi^{n-1}\delta_\xi + (\eta_y^2)^n\phi_\eta^{n-1}\delta_\eta\right](\phi^n - \phi^{n-1}) \\
&\quad + \Delta t(J^{n+1}/\beta^n)\{(\hat{\rho}^n - \hat{\rho}^{n-1}) + h\bar{\delta}_\xi(\xi_x^2/J)^{n+1}\rho^n\bar{\delta}_\xi\phi^n \\
&\quad + h\bar{\delta}_\eta(\eta_y^2/J)^{n+1}\rho^n\bar{\delta}_\eta\phi^n\}
\end{aligned} \tag{31}$$

This equation has the form

$$L_\eta L_\xi (\phi^{n+1} - \phi^n) = R \tag{28}$$

and is implemented as an algorithm as

$$L_\eta \Delta\phi^* = R \tag{29}$$

$$L_\xi \Delta\phi^n = \Delta\phi^*$$

$$\phi^{n+1} = \phi^n + \Delta\phi^n$$

This algorithm requires only a series of scalar tridiagonal inversions and it is therefore very efficiently implemented. Computer storage equivalent to four levels of $\phi$ have to be supplied with $\rho$ computed from the Bernoulli equation as needed.

## RESULTS AND APPLICATIONS

Although the various finite difference issues are very similar for the unsteady small disturbance and full potential methods, there is a large difference in the extent to which these methods have been developed and applied. Naturally, this difference reflects the relative complexity of the two methods.

One of the most interesting test computations demonstrating the use of unsteady potential finite difference methods concerns the flow about a pulsating airfoil (that is, one having a time-varying thickness). Although the idea of a pulsating airfoil seems farfetched, it can be shown by considering the two-dimensional small disturbance equation to emulate a time-varying free-stream Mach number. And free-stream Mach number-variation does occur for an advancing helicopter rotor. Now consider a parabolic arc airfoil whose mid-chord thickness varies as

$$\tau(t) = \begin{cases} 0.1[\,10 - t + 6(t/15)^2](t/15)^3 , & 0 \le t \le 15 \\ 0.1\left[10 - 15\left(\dfrac{30-t}{15}\right) + 6\left(\dfrac{30-t}{15}\right)^2\right]\left(\dfrac{30-t}{15}\right)^3 , & 15 \le t \le 30 \\ 0 , & t \ge 30 \end{cases}$$

where $t = t'U_\infty/\ell$ and is nondimensionalized by chord lengths traveled. Since the variation takes place over many chords of travel it is suitable to invoke the low frequency approximation for the small disturbance equation — that is, all time derivatives except $\phi_{xt}$ are ignored in Eq. (7). (Physically, ignoring $\phi_{tt}$ in Eq. (7) amounts to assuming an infinite downstream propagation rate.) Figures 2 and 3 show a comparison of the resulting flow computed by the full potential method (Goorjian, Ref. 9) and the low frequency small disturbance equation (Ballhaus and Steger, Ref. 23). When the airfoil is thinning it becomes subcritical by propagating the shock upstream from the leading edge. The two approaches

give essentially the same result. The most significant difference between the two computations is perhaps the greater dissipation of the forward propagating shock for the full potential case. This can be controlled by the choice of upstream density biasing function. For this case, density switching was employed. Recall that it is possible to use an unswitched upstream density as long as a higher order difference is used to maintain accuracy. This is demonstrated in Fig. 4 which compares switched and unswitched density biasing for the computation of the steady flow on a biconvex profile.

The previously mentioned shock motion is so different from our previous experience that it demands some kind of experimental study. By coincidence, such a study was performed by Tijdeman and his associates (24,25) at NLR, the Netherlands, at the same time that the first of these computations was being done. They acquired detailed flow visualization and loading data for a NACA64A006 airfoil with an oscillating flap. They delineated three basic types of shock motion caused by the oscillating flap. These are:

1. Type A. The shock moves nearly sinusoidally (only the lowest harmonic was measured) with a phase shift relative to the flap motion. The shock strength varies, being a minimum while moving downstream and a maximum while moving upstream.
2. Type B. This case is similar to Type A except that the shock strength variation disappears during the downstream moving portion of its cycle.
3. Type C. At slightly supercritical conditions there is no supersonic region for a large portion of the flap cycle. In this case the airfoil becomes subcritical by propagating the shock upstream off of the leading edge. There is no downstream shock motion.

The ability of potential methods to compute these shock motions was demonstrated by Ballhaus and Goorjian (26). In this work, two-dimensional finite difference solutions of the low frequency small disturbance equation were obtained by the ADI approach (program, LTRAN2). The computed Type B motion is shown in Fig. 5. The shock-motion disappearance and reappearance are shown here for LTRAN2 and the Magnus-Yoshihara code (an isentropic Euler code). Type C motion is illustrated in Fig. 6. In the succession of plots shown, the shock is seen to form at mid-chord and move upstream until it disappears at the leading edge. The shock is seen to disappear here rather than visibly propagate upstream as in Fig. 3, probably due to numerical dissipation. It is interesting that the conditions for which these various types of shock motion were computed do not compare well with the actual experimental conditions. It is generally felt now (on the basis of comparing different codes and of computations of wall effects) that the discrepancy is due to tunnel-wall and possibly viscous effects rather than numerical problems. Nevertheless, the fact that experiment and computation produce the same kinds of phenomena greatly increases the significance of both.

A primary application of unsteady transonic potential methods is in the prediction of loads on helicopter rotors in forward flight. Although aeroelastic effects are important, in this case the main source of unsteadiness is in the flow itself. The most notable distinction between

the fixed and rotary wing is that for the latter the free stream (in body-fixed coordinates) is constantly accelerating and decelerating. That is, the rotor "sees" the free-stream Mach number to be periodically varying. The reduced frequency of this variation is the inverse of the blade aspect ratio. Since aspect ratio is of the order of 10 for a rotor, it is possible to invoke the low frequency approximation. The effectiveness of the small disturbance potential methods has been demonstrated by comparison of computed flows with measured surface pressure on a nonlifting rotor blade. Figures 7 and 8 demonstrate this comparison at two blade azimuths, $\psi = 60^\circ$ and $120^\circ$, respectively (see Fig. 7 for definition of azimuth angle). Measurements and computations are in excellent agreement. The effects of unsteadiness are evident in this figure because for the two azimuths shown the chordwise Mach numbers are identical. Yet the pressures are quite different. There are no shocks seen at $\psi = 60^\circ$, but they are evident at $120^\circ$. This azimuthal shock asymmetry is not explainable by cross-flow effects, because the inboard station is too far from the tip. Furthermore, the inboard results can be readily obtained by two-dimensional computations (27). Very often, the shock motion in these rotor computations appears to be Type C, the upstream propagating type. This is seen in Fig. 9 (27) which shows a low frequency small disturbance two-dimensional computation of a lifting rotor flow. In this case the blade is oscillating and also sees a varying free-stream Mach number. The flow on the bottom surface of the airfoil is seen to return to subcritical conditions by propagating the shock upstream.

The most fascinating feature of the above computations is that they are so easy to perform compared with wind-tunnel testing. Yet they have often proven to contain most of the essential physics. In the following discussion we shall demonstrate the use of a potential computation as a "numerical wind tunnel" to explore a little-studied but possibly very important problem.

An unusual unsteady flow feature of helicopter rotors is that they are never very far from the tip vortex of a preceding blade and close blade/vortex interactions often occur. Under certain conditions a blade can encounter a vortex which is nearly parallel to itself. Such encounters are an important noise source and require modeling. An extremely simple model is provided by a two-dimensional small disturbance computation of a near-vortex encounter. The time scale for this problem ($\ell/U_\infty$) is very brief and it is necessary to include all time derivatives. The vortex is introduced as the edge of a potential discontinuity sheet (Fig. 10) which is stepped through the computational grid. The vortex is moved through the grid in a prescribed straight line at the undisturbed flow speed. The strength of the vortex is given as an effective lift coefficient, $C_{LV}$, of an airfoil having the same circulation as the vortex. Note that while the sheet describing the vortex in Fig. 10 is horizontal, its direction is irrelevant. The effect of unsteadiness in these computations is shown in Fig. 11, which compares blade surface pressure distributions for a fixed and moving vortex (the vortex, located at mid-chord and 0.96 chords below the blade, has the strength, $C_{LV} = 0.1$). There is no apparent disturbance for the unsteady moving vortex case but a large disturbance for the steady case. This result undoubtedly reflects the fact that the vortex exerts no force on

the fluid in the unsteady case. In fact, in order to get a sizeable effect on the surface pressures (other than the expected angle-of-attack variation) it is necessary to bring the vortex quite close to the blade and increase its strength. Figure 12 shows the lift variation for a blade with a vortex of strength $C_{LV} = 0.4$ whose path lies 0.25 chords beneath the blade. As the vortex passes it induces a shock on the bottom surface. This shock disappears very suddenly with no obvious upstream propagation. Through all this activity the upper surface seems curiously unaffected.

The importance of such a computational experiment is difficult to assess because many liberties have been taken. Nevertheless, it is clear that the neglect of unsteadiness would be to greatly overestimate the effects of these phenomena. For sufficiently strong or close vortices, large and rapid bottom surface disturbances can be computed and these must have acoustic significance. However, this could be mitigated by allowing the vortex to move freely rather than follow a fixed path. Undoubtedly, an assessment of these sorts of computations cannot be made without some experiments. Thus it seems that the effect of the "numerical wind tunnel" can be to guide the use of and increase the need for the physical wind tunnel.

## CONCLUDING REMARKS

This paper has made no attempt to treat unsteady potential finite difference methods exhaustively or in great detail. Rather, a typical small disturbance method, and a full potential method have been discussed in parallel in the context of the issues (choice of equations and boundary conditions, linearizations, discretizations, and algorithms) which arise in all code development. One can discuss a typical method because the choices taken in code development are quite few. For instance, the choice in the equations centers around whether one wishes to have one or two dependent variables. Linearizations and discretizations vary little. All methods employ some sort of upstream biasing and nearly the same time discretizations. Algorithm development always comes down to some sort of approximate factorization. In short, although there is much development work to be done, the general area of potential finite difference methods is beginning to mature quite nicely. We shall surely see the development of several practical three-dimensional unsteady full potential codes within the coming year or two.

There remains one vital issue which has not been covered in this discussion: the subject of grid generation. On this point finite difference methods are often more of an art than a science. The problem is not as much to generate a mesh as to know the effect of this mesh on a particular problem and solution method. This is especially difficult in the unsteady case where we may have the presence of moving flow features (shocks and vortices) which require resolution. It is ironic that while gridding is the most fundamental feature of finite difference methods, the topic of grids remains to be organized into an organic and systematic entity. The requirements for large-scale unsteady computations must certainly change this situation, because they will require fast, automatic, and reliable grid schemes.

REFERENCES

1. J. L. Steger and B. S. Baldwin, "Shock Waves and Drag in the Numerical Calculation of Isentropic Transonic Flow," NASA TN D-6997, Oct. 1972.

2. J. vander Vooren and J. W. Sloof, "On Inviscid Isentropic Flow Models Used for Finite Difference Calculations of Two-Dimensional Transonic Flows with Embedded Shocks About Airfoils," NLR MP 73024U.

3. M. P. Isom, "Unsteady Subsonic and Transonic Potential Flow Over Helicopter Rotor Blades," NASA CR-2463, Oct. 1974.

4. J. vander Vooren, J. W. Sloof, G. H. Huizing, and A. van Essen, "Remarks on the Suitability of Various Transonic Small Perturbation Equations to Describe Three-Dimensional Transonic Flow," presented at Proc. Symposium Transonicum II, 1975.

5. D. Kwak, "Non-Reflecting Far-Field Boundary Conditions for Unsteady Transonic Flow Computation," AIAA-80-1393, presented at the AIAA Fluid and Plasma Dynamics Conference, Snowmass, CO., July 14-16, 1980.

6. B. Engquist and A. Majda, "Absorbing Boundary Conditions for the Numerical Simulation of Waves," Math. Comp., Vol. 31, No. 139, July 1977, pp. 629-651.

7. B. Engquist and A. Majda, "Radiation Boundary Conditions for Acoustic and Elastic Wave Calculations," Comm. Pure and Applied Math., Vol. 32, May 1979, pp. 313-357.

8. B. Engquist and A. Majda, "Numerical Radiation Boundary Conditions for Unsteady Transonic Flow," Journal of Comp. Phys., Vol. 40, April 1981, pp. 91-103.

9. P. M. Goorjian, "Implicit Computations of Unsteady Transonic Flow Governed by the Full Potential Equation in Conservation Form," AIAA-80-0150, presented at the AIAA 18th Aerospace Sciences Meeting, Pasadena, CA., Jan. 14-16, 1980.

10. J. L. Steger and F. X. Caradonna, "A Conservative Implicit Finite Difference Algorithm for the Unsteady Transonic Full Potential Equation," AIAA-80-1368, presented at the AIAA 13th Fluid and Plasma Dynamics Conference, Snowmass, CO., July 14-16, 1980.

11. R. Chipman and A. Jameson, "Alternating Direction Implicit Algorithm for Unsteady Potential Flow," AIAA Journal, Vol. 20, No. 1, Jan. 1982.

12. E. M. Murman and J. D. Cole, "Calculation of Plane Steady Transonic Flows," AIAA Journal, Vol. 9, No. 1, 1971, pp. 114-121.

13. F. X. Caradonna and J. L. Steger," Implicit Potential Methods for the Solution of Transonic Rotor Flows," ARO report 80-3, Proceedings of the 1980 Army Numerical Analysis and Computers Conference.

14. E. M. Murman and J. D. Cole, "Inviscid Drag at Transonic Speeds," presented at the AIAA 7th Fluid and Plasma Dynamics Conference, Palo Alto, California, July 1973, pp. 27-40.

15. K. Isogai, "Calculation of Unsteady Transonic Flow Over Oscillating Airfoils Using the Full Potential Equation," AIAA-77-448, presented at the AIAA Dynamics Specialist Conference, San Diego, CA., Mar. 24-25, 1977.

16. I-Chung Chang, "Unsteady Transonic Flow Past Airfoils in Rigid Body Motion," DOE/ER/03077-170, Courant Institute of Mathematical Sciences, Mar. 1981.

17. T. L. Holst and W. F. Ballhaus, "Fast Conservative Schemes for the Full Potential Equation Applied to Transonic Flows," AIAA Journal, Vol. 17, No. 2, Feb. 1979, pp. 145-152.

18. A. Jameson, "Transonic Potential Flow Calculations Using Conservative Form," AIAA Second Computational Fluid Dynamics Conference Proceedings, June 1975, pp. 148-155.

19. M. Hafez, J. South, and E. Murman, "Artifical Compressibility Methods for Numerical Solutions of the Transonic Full Potential Equation," AIAA Journal, Vol. 17, Aug. 1979, pp. 838-844.

20. J. J. Chattot, "Calculation of Three-Dimensional Unsteady Transonic Flows Past Helicopter Blades," NASA Technical Paper 1721, Oct. 1980.

21. J. J. Philippe and J. J. Chattot, "Experimental and Theoretical Studies on Helicopter Blade Tips at ONERA," Paper No. 46, presented at the Sixth European Rotorcraft and Powered Lift Aircraft Forum, Bristol, U.K., Sept. 1980, pp. 16-19.

22. D. P. Rizzetta and W. C. Chin, "Effect of Frequency in Unsteady Transonic Flow," AIAA Journal, Vol. 17, No. 7, July 1979, pp. 779-781.

23. W. F. Ballhaus and J. L. Steger, "Implicit Approximate-Factorization Schemes for the Low-Frequency Transonic Equation," NASA TM X-73,082, Nov. 1975.

24. H. Tijdeman, "Investigations of the Transonic Flow Around Oscillating Airfoils," Ph.D. Thesis, National Aerospace Laboratory (Netherlands), TR 77090, Oct. 1977.

25. H. Tijdeman, P. Schippers, and A. J. Persoon, "Unsteady Airloads on an Oscillating Supercritical Airfoil," AGARD CP-226, Unsteady Airloads in Separated and Transonic Flow, Apr. 1977.

26. W. F. Ballhaus and P. M. Goorjian, "Implicit Finite-Difference Computations of Unsteady Transonic Flows About Airfoils, Including the Treatment of Irregular Shock-Wave Motions," AIAA Journal, Vol. 15, No. 12, Dec. 1977, pp. 1728-1735.

27. F. X. Caradonna and J. J. Philippe, "The Flow Over a Helicopter Blade Tip in the Transonic Regime," Vertica, Vol. 2, 1978, pp. 43-60.

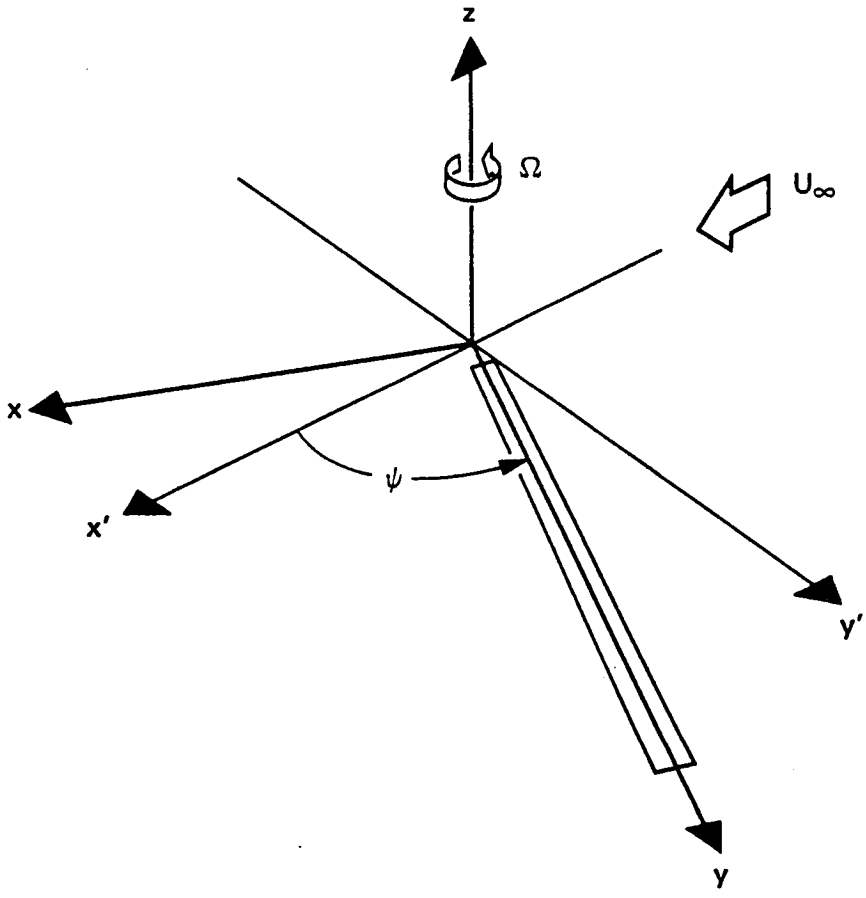


Fig. 1 - Rotating and translating coordinate system

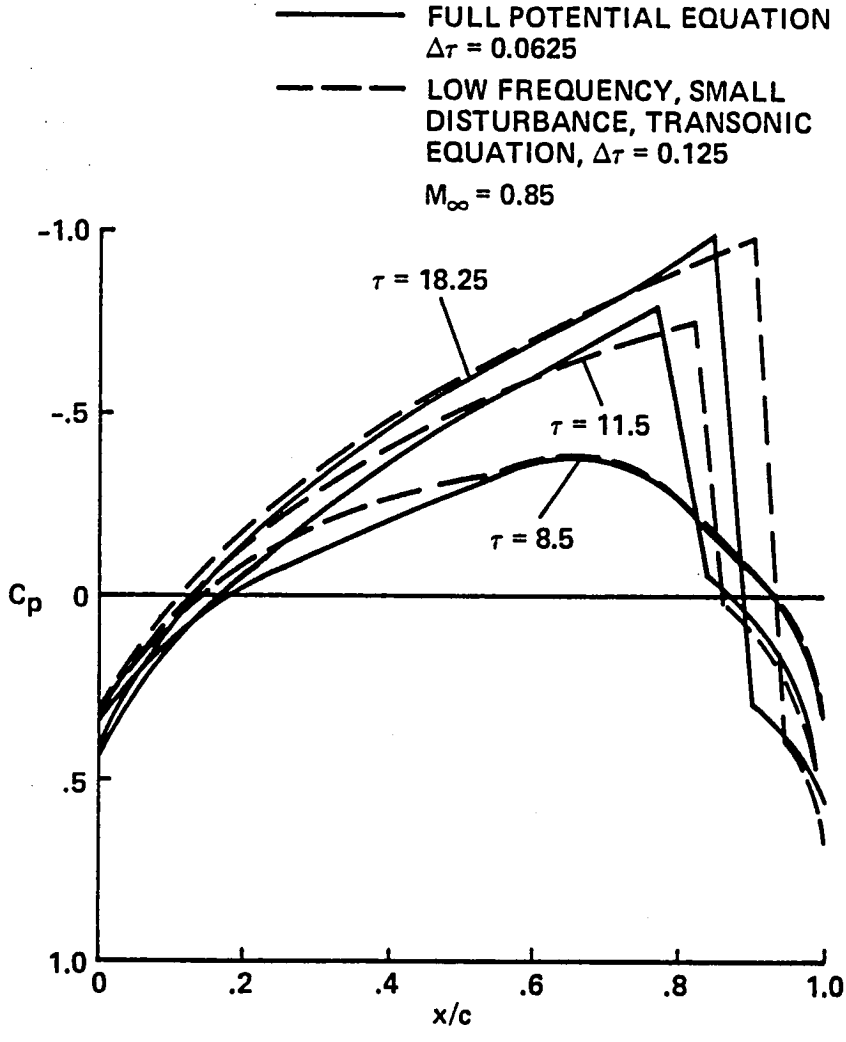


Fig. 2 - Pressure variation on a pulsating airfoil--airfoil thickening

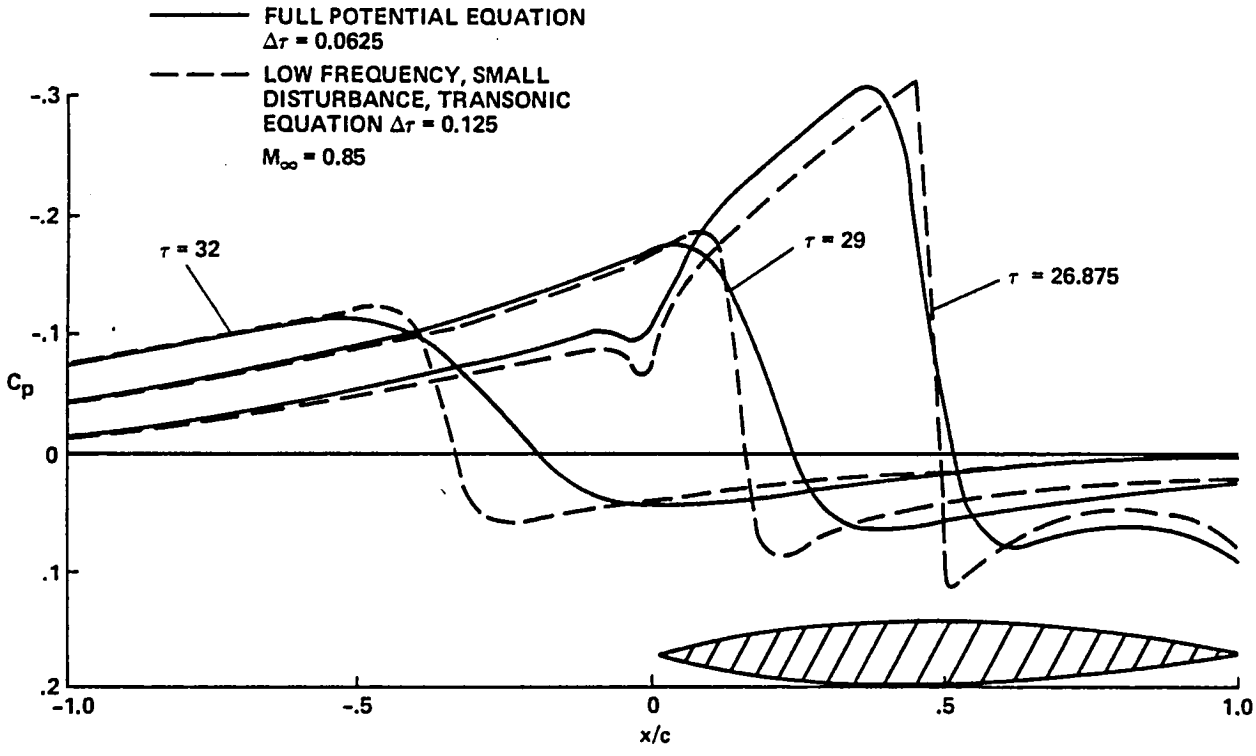


Fig. 3 - Pressure variation on a pulsating airfoil--airfoil thinning

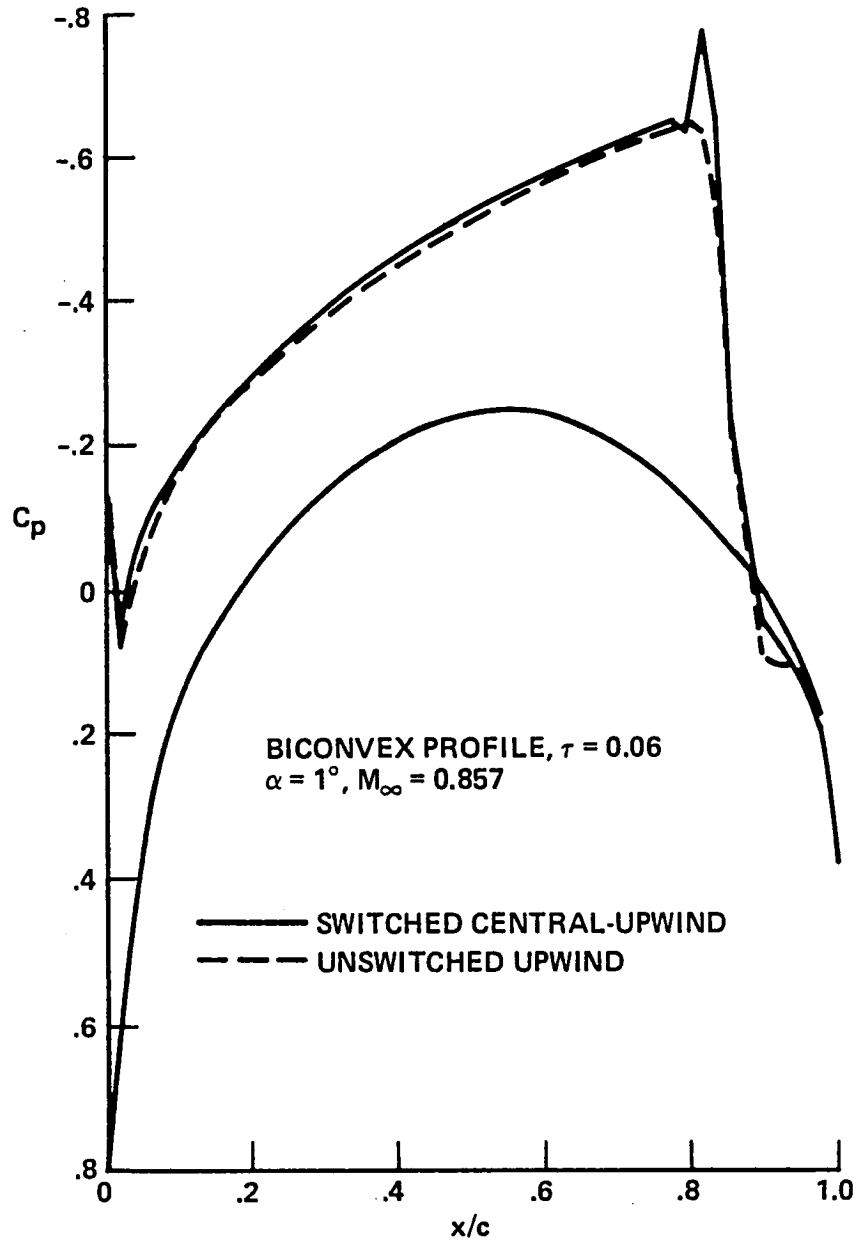


Fig. 4 - A comparison of switched and unswitched density biasing for a full potential computation

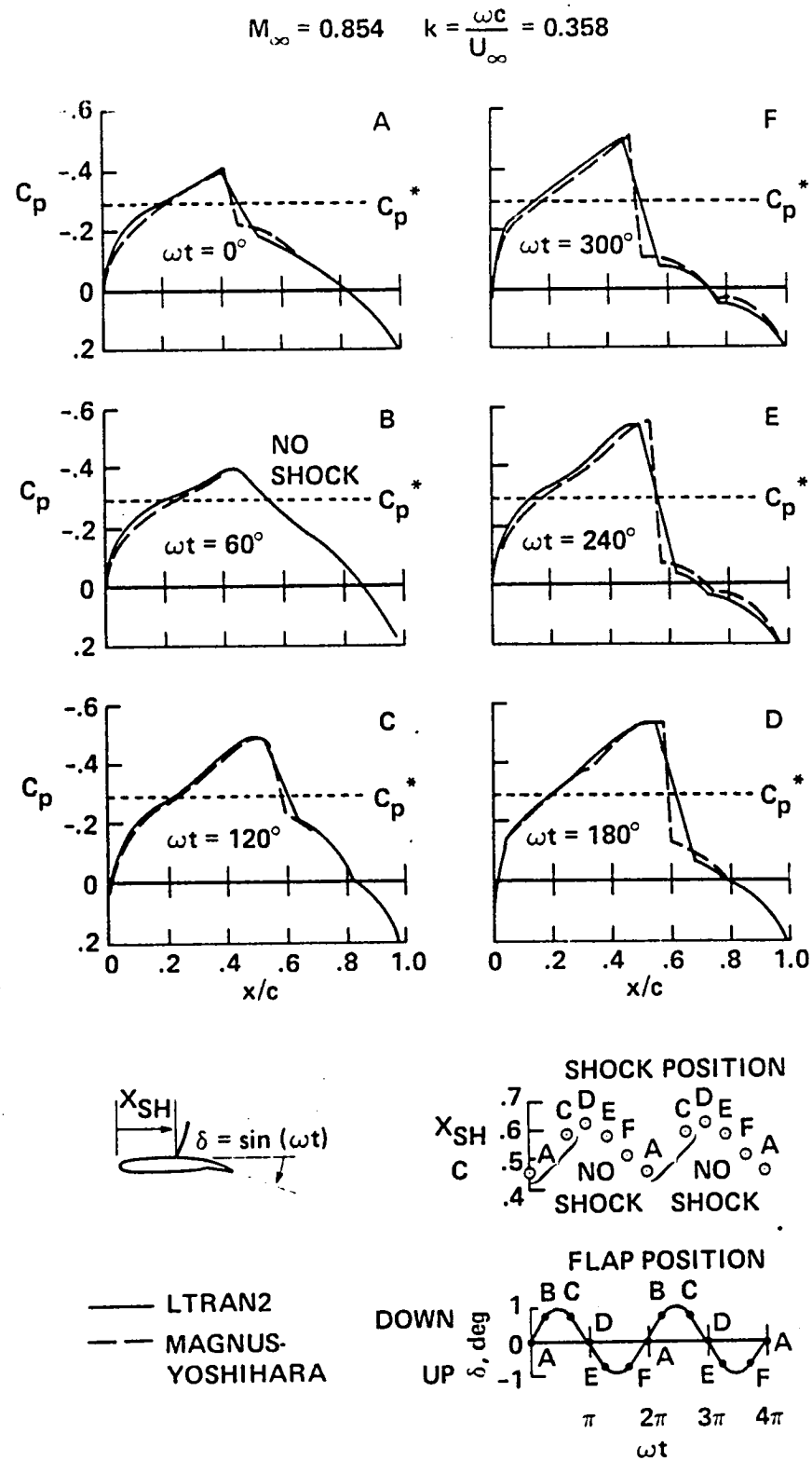


Fig. 5 - Unsteady upper surface pressure variation for a NACA64A006 airfoil with an oscillating flap, Type B motion

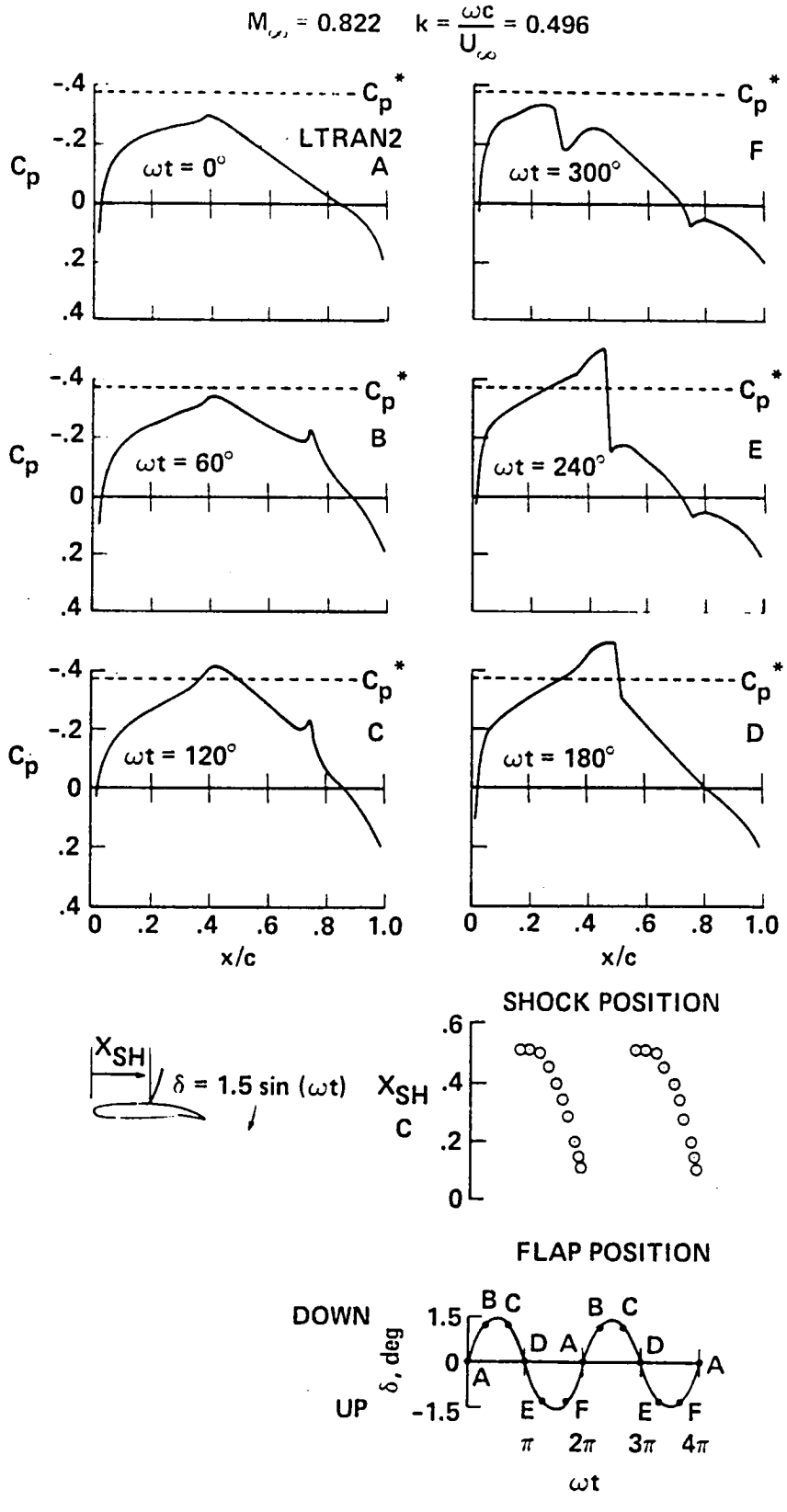


Fig. 6 - Unsteady upper surface pressure variation for a NACA64A006 airfoil with an oscillating flap, Type C motion

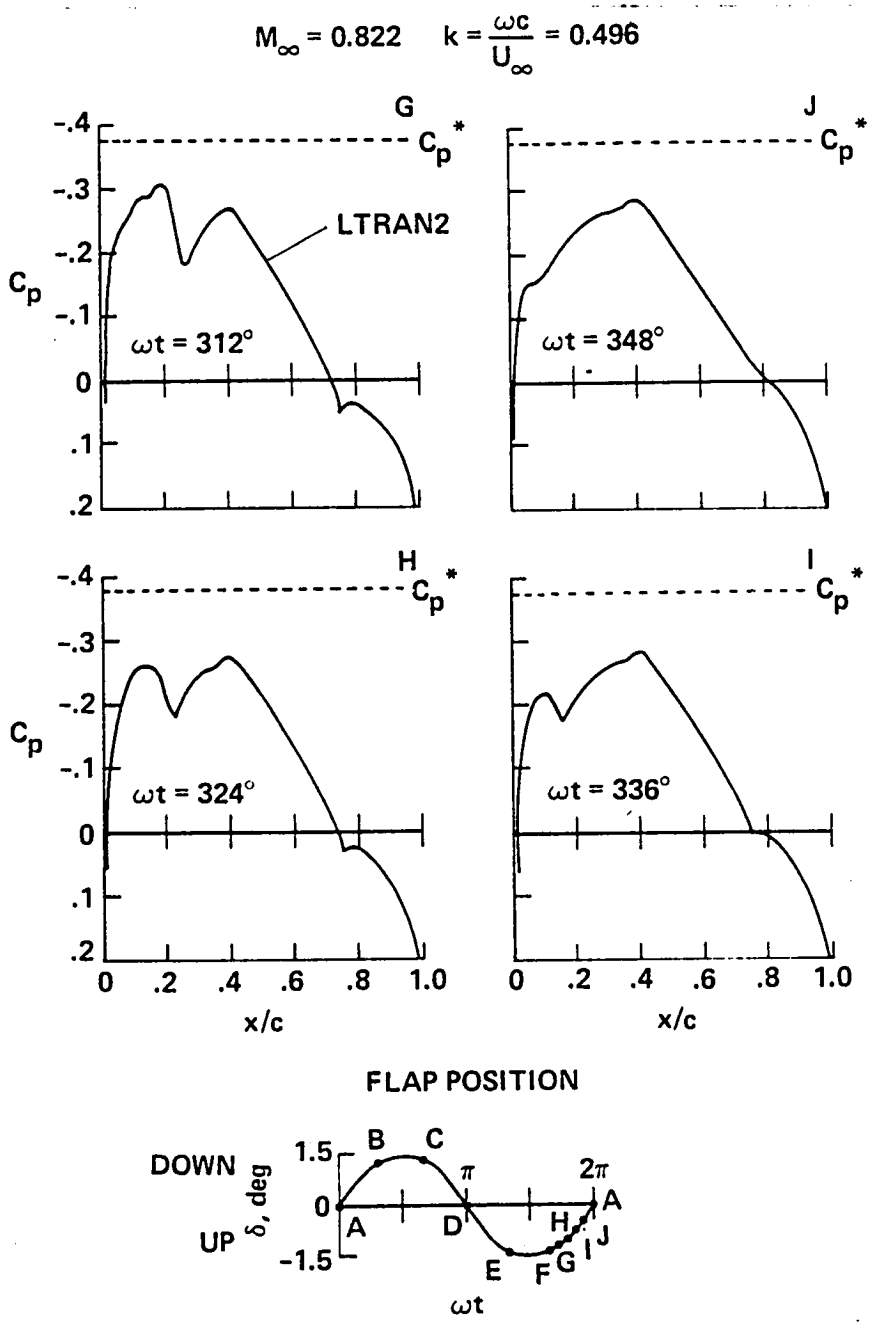


Fig. 6 - Concluded

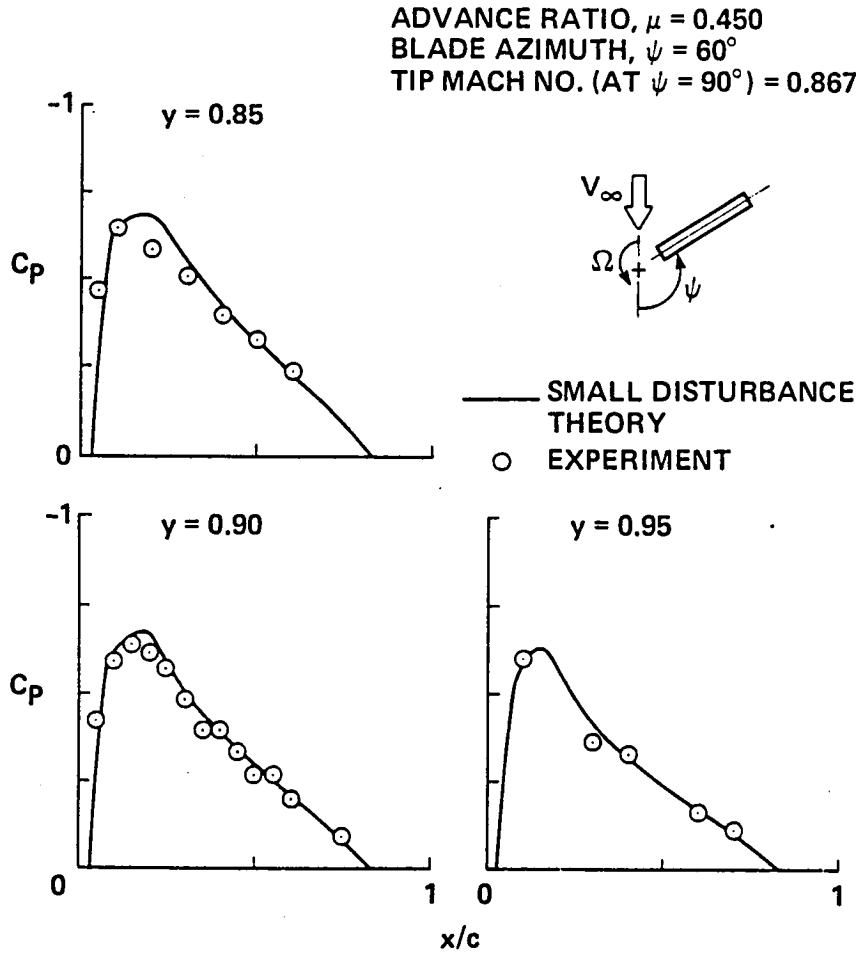


Fig. 7 - Measured and computed pressure distribution on an advancing, nonlifting rotor--60° blade azimuth

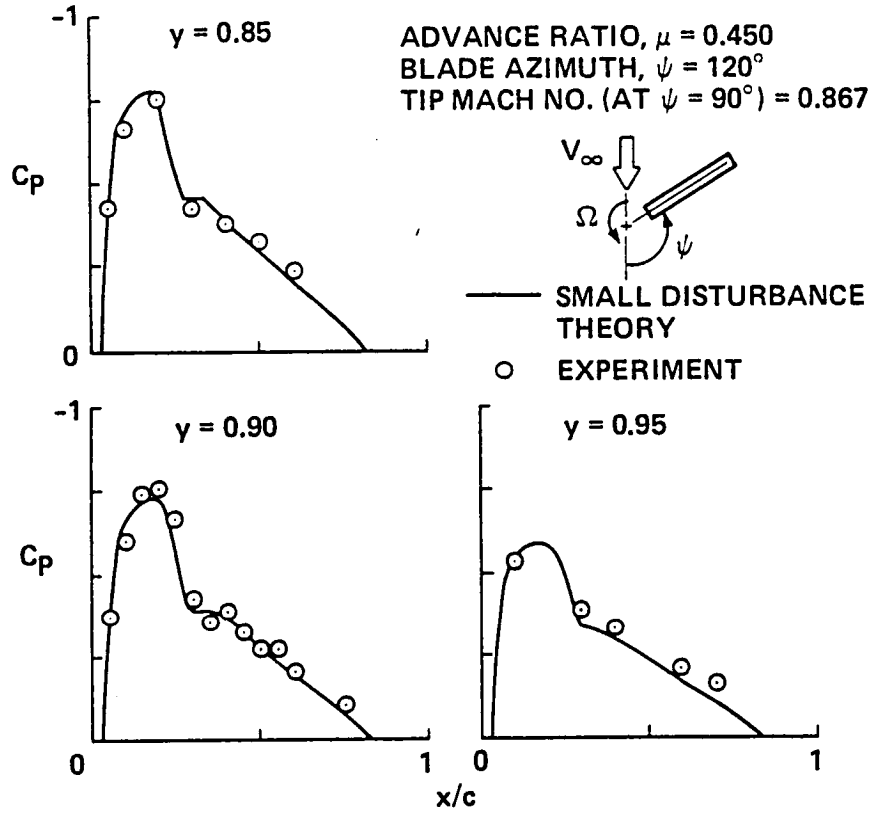


Fig. 8 - Measured and computed pressure distribution on an advancing, nonlifting rotor--120° blade azimuth

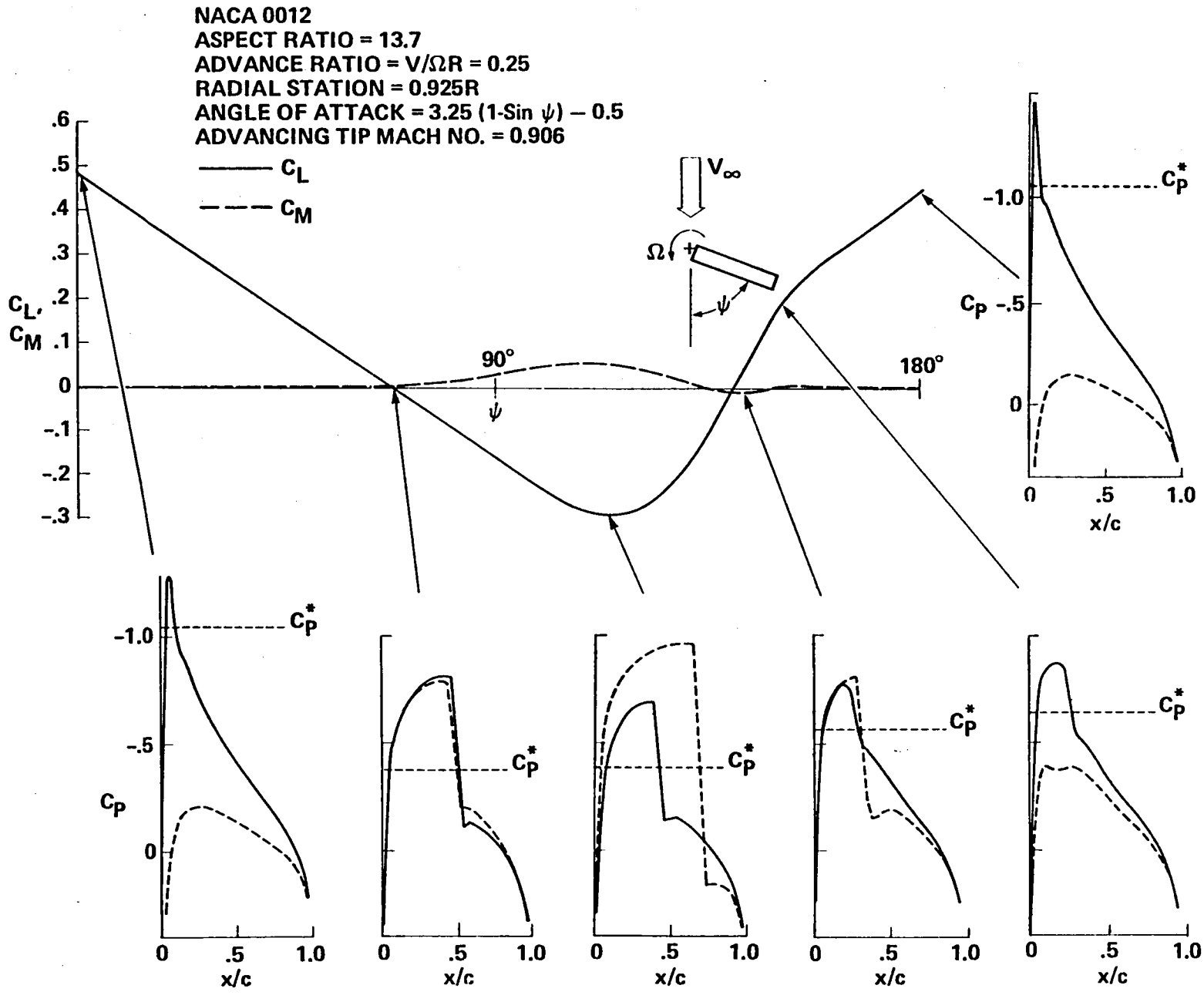


Fig. 9 - Computed load variation on a helicopter rotor

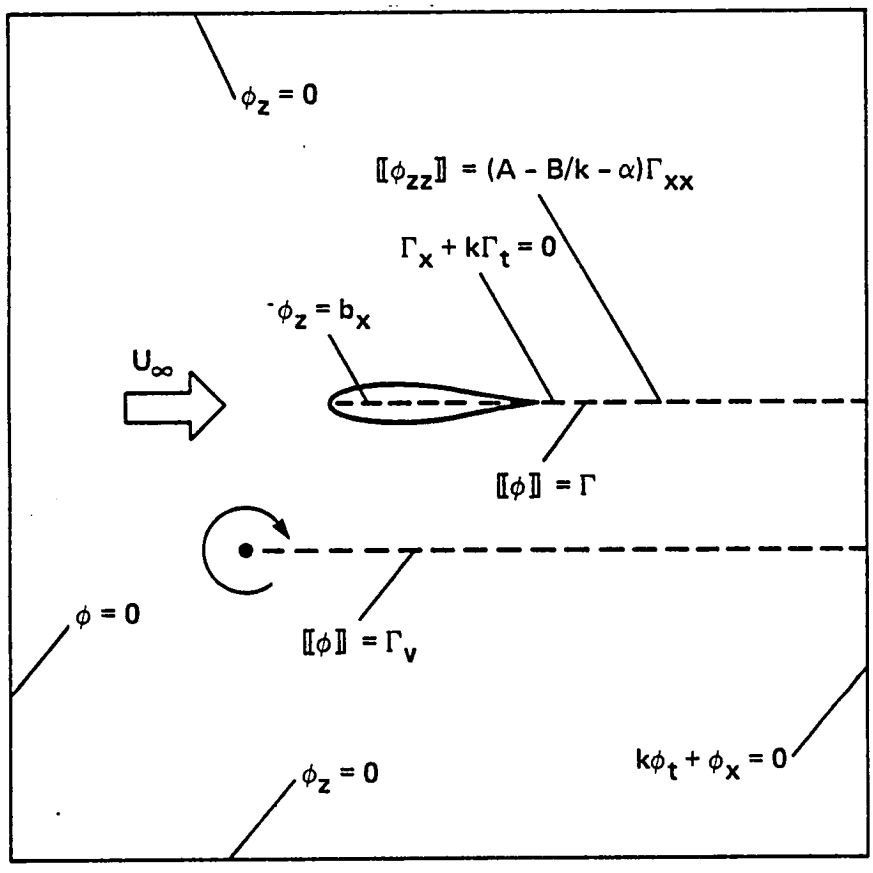


Fig. 10 - Boundary conditions for the blade/vortex interaction problem

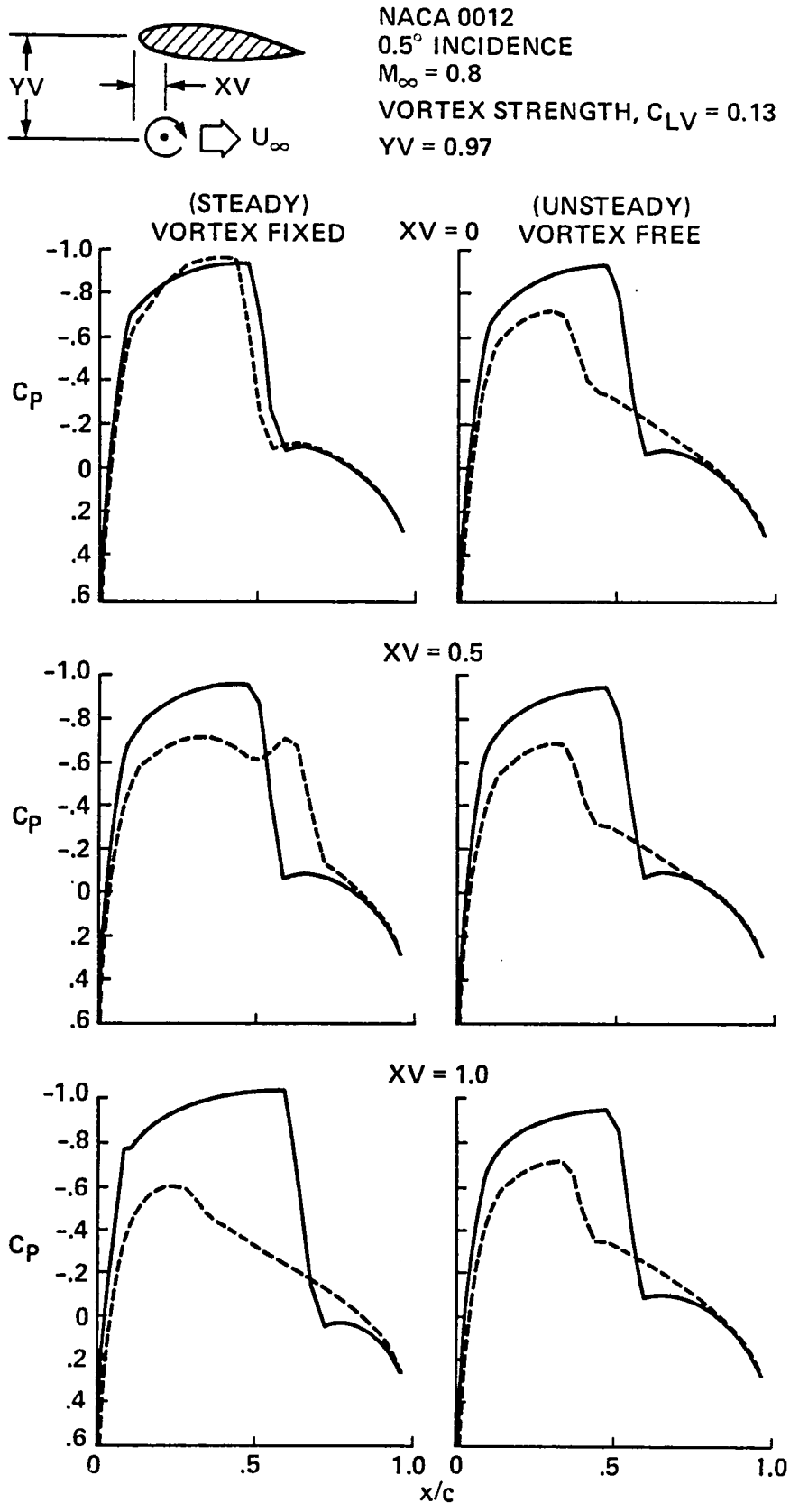


Fig. 11 - Steady and unsteady flow computations for the blade/vortex interaction problem

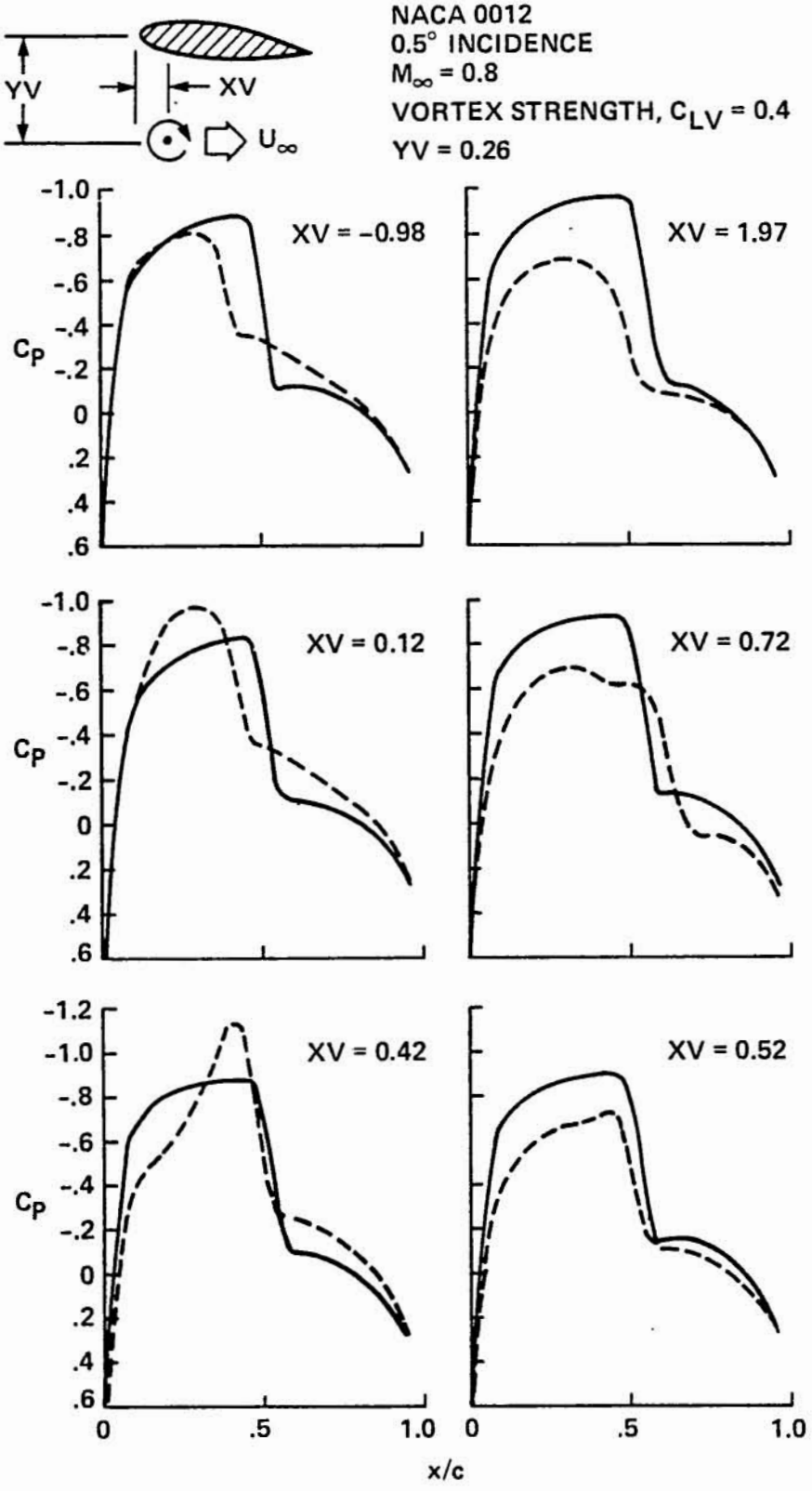


Fig. 12 - Unsteady flow computations for the blade/vortex interaction problem

| 1. Report No. NASA TM-84248<br>AVRADCOM Tech. Rep. 82-A-7 | 2. Government Accession No. | 3. Recipient's Catalog No. |
|---|---|---|
| 4. Title and Subtitle<br>FINITE DIFFERENCE METHODS FOR THE SOLUTION OF UNSTEADY POTENTIAL FLOWS | | 5. Report Date<br>6. Performing Organization Code<br>A-8942 |
| 7. Author(s)<br>F. X. Caradonna | | 8. Performing Organization Report No.<br>10. Work Unit No.<br>K-1585 |
| 9. Performing Organization Name and Address<br>NASA Ames Research Center and Headquarters<br>Army Research and Technology Laboratories<br>(AVRADCOM), Moffett Field, CA 94035 | | 11. Contract or Grant No.<br>13. Type of Report and Period Covered<br>Technical Memorandum |
| 12. Sponsoring Agency Name and Address<br>National Aeronautics and Space Administration,<br>Washington, D.C. 20546, and U.S. Army Aviation<br>Research & Development Command, St. Louis, MO. 63116 | | 14. Sponsoring Agency Code<br>992-21-01 |

15. Supplementary Notes

Point of Contact: F. X. Caradonna, Ames Research Center, MS-215-1, Moffett Field, CA 94035. (415) 965-6062 or FTS 448-6062.

16. Abstract

A brief review is presented of various problems which are confronted in the development of an unsteady finite difference potential code. This review is conducted mainly in the context of what is done for a typical small disturbance and full potential method. The issues discussed include choice of equations, linearization and conservation, differencing schemes, and algorithm development. A number of applications, including unsteady three-dimensional rotor calculations, are demonstrated.

| 17. Key Words (Suggested by Author(s)) | 18. Distribution Statement |
|---|---|
| unsteady, transonic, potential methods, finite difference methods | Unlimited<br>Subject Category: 01 |

| 19. Security Classif. (of this report) | 20. Security Classif. (of this page) | 21. No. of Pages | 22. Price* |
|---|---|---|---|
| Unclassified | Unclassified | 36 | A03 |

*For sale by the National Technical Information Service, Springfield, Virginia 22161